Article

Cell Stem Cell

Myocardial Infarction Activates CCR2$^+$ Hematopoietic Stem and Progenitor Cells

Graphical Abstract

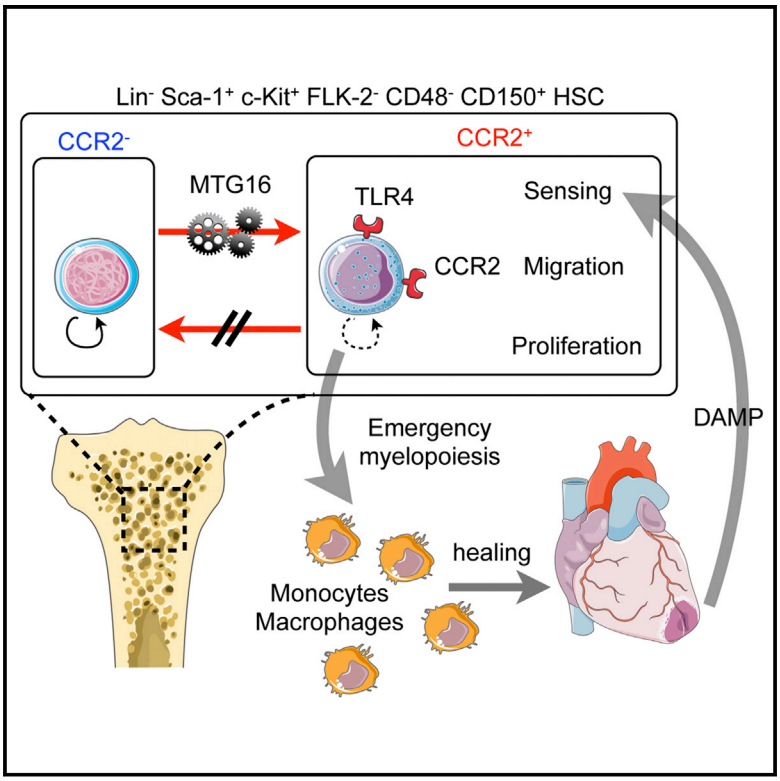

Authors

Partha Dutta, Hendrik B. Sager, ..., Ralph Weissleder, Matthias Nahrendorf

Correspondence

dutta.partha@mgh.harvard.edu (P.D.), mnahrendorf@mgh.harvard.edu (M.N.)

In Brief

Blood leukocyte levels predict mortality following myocardial infarction (MI), but the cellular mechanisms leading to this increase are unclear. Dutta et al. show that CCR2 expression defines an upstream subset of HSPCs that proliferate, migrate, and generate myeloid cells following ischemic injury, and their absence is associated with decreased healing.

Highlights

- CCR2 expression identifies an HSPC subset that responds vigorously to ischemia
- Myeloid translocation gene 16 (*Mtg16*) is necessary for the emergence of CCR2$^+$ HSPCs
- Absence of CCR2$^+$ HSPCs associates with compromised infarct healing
- CCR2$^+$CD150$^+$CD48$^-$ LSKs preferentially migrate outside of the bone marrow

Accession Numbers

GSE53827

Dutta et al., 2015, Cell Stem Cell *16*, 477–487
May 7, 2015
http://dx.doi.org/10.1016/j.stem.2015.04.008

CellPress

Cell Stem Cell
Article

Myocardial Infarction Activates CCR2$^+$ Hematopoietic Stem and Progenitor Cells

Partha Dutta,[1,11,*] Hendrik B. Sager,[1,11] Kristy R. Stengel,[2] Kamila Naxerova,[3] Gabriel Courties,[1] Borja Saez,[4] Lev Silberstein,[4] Timo Heidt,[1] Matthew Sebas,[1] Yuan Sun,[1] Gregory Wojtkiewicz,[1] Paolo Fumene Feruglio,[1] Kevin King,[1] Joshua N. Baker,[5] Anja M. van der Laan,[6] Anna Borodovsky,[7] Kevin Fitzgerald,[7] Maarten Hulsmans,[1] Friedrich Hoyer,[1] Yoshiko Iwamoto,[1] Claudio Vinegoni,[1] Dennis Brown,[1] Marcelo Di Carli,[8] Peter Libby,[9] Scott W. Hiebert,[2] David T. Scadden,[4] Filip K. Swirski,[1] Ralph Weissleder,[1,10] and Matthias Nahrendorf[1,*]

[1]Center for Systems Biology, Massachusetts General Hospital and Harvard Medical School, Simches Research Building, 185 Cambridge Street, Boston, MA 02114, USA

[2]Department of Biochemistry, Vanderbilt School of Medicine, Nashville, TN 37235, USA

[3]Edwin L. Steele Laboratory, Department of Radiation Oncology, Massachusetts General Hospital, 55 Fruit Street, Boston, MA 02144, USA

[4]Center for Regenerative Medicine, Massachusetts General Hospital, Simches Research Building, 185 Cambridge Street, Boston, MA 02114, USA

[5]Department of Cardiac Surgery, Massachusetts General Hospital, 55 Fruit Street, Boston, MA 02144, USA

[6]Department of Cardiology, Academic Medical Center, University of Amsterdam, P.O. Box 22660, Amsterdam, the Netherlands

[7]Alnylam Pharmaceuticals, 300 Third Street, Cambridge, MA 02142, USA

[8]Division of Nuclear Medicine and Molecular Imaging, Department of Radiology, Brigham and Women's Hospital, 75 Francis Street, Boston, MA 02115, USA

[9]Cardiovascular Division, Department of Medicine, Brigham and Women's Hospital, 75 Francis Street, Boston, MA 02115, USA

[10]Department of Systems Biology, Harvard Medical School, 200 Longwood Avenue, Boston, MA 02115, USA

[11]Co-first author

*Correspondence: dutta.partha@mgh.harvard.edu (P.D.), mnahrendorf@mgh.harvard.edu (M.N.)

http://dx.doi.org/10.1016/j.stem.2015.04.008

SUMMARY

Following myocardial infarction (MI), myeloid cells derived from the hematopoietic system drive a sharp increase in systemic leukocyte levels that correlates closely with mortality. The origin of these myeloid cells, and the response of hematopoietic stem and progenitor cells (HSPCs) to MI, however, is unclear. Here, we identify a CCR2$^+$CD150$^+$CD48$^-$ LSK hematopoietic subset as the most upstream contributor to emergency myelopoiesis after ischemic organ injury. This subset has 4-fold higher proliferation rates than CCR2$^-$CD150$^+$CD48$^-$ LSK cells, displays a myeloid differentiation bias, and dominates the migratory HSPC population. We further demonstrate that the myeloid translocation gene 16 (*Mtg16*) regulates CCR2$^+$ HSPC emergence. *Mtg16*$^{-/-}$ mice have decreased levels of systemic monocytes and infarct-associated macrophages and display compromised tissue healing and post-MI heart failure. Together, these data provide insights into regulation of emergency hematopoiesis after ischemic injury and identify potential therapeutic targets to modulate leukocyte output after MI.

INTRODUCTION

Leukocytes, especially monocytes and macrophages, participate integrally in all stages of ischemic heart disease (Moore and Tabas, 2011; Swirski and Nahrendorf, 2013). During atherogenesis, bone-marrow-derived monocytes enter the vessel wall and give rise to macrophages and foam cells with tissue-destructive properties (Libby, 2002). Once a plaque ruptures, leukocytes massively accumulate in ischemic heart tissue, where they promote healing but may also worsen tissue damage if supplied in exaggerated numbers. An increase in circulating white cells promotes atherosclerosis, and myocardial infarction (MI) causes acute leukocytosis, which correlates closely with cardiovascular mortality (Swirski and Nahrendorf, 2013). How organ ischemia activates the hematopoietic system is poorly understood.

The majority of hematopoietic stem cells (HSCs) are quiescent and enter the cell cycle only sparingly to self-renew and produce progeny (Wilson et al., 2008). Even though most HSCs are dormant at any given time point, they can be activated by a systemic insult such as infection (Essers et al., 2009; Baldridge et al., 2010; Takizawa et al., 2011). Moreover, HSCs are able to reversibly change between quiescence and proliferation states (Glauche et al., 2009). However, an "effector subset" that drives the proliferation response after a systemic insult has not been identified. We do not know how HSCs respond to MI, which is the most common cause of death. The HSC response to tissue injury may be of particular relevance to patients that survive an ischemic insult because myeloid progeny play a major role in tissue repair and patient recovery (Swirski and Nahrendorf, 2013). Here we describe a CD150$^+$CD48$^-$Lineage$^-$Sca-1$^+$c-Kit$^+$ (LSK) subset that can be identified by flow cytometry staining for the chemokine receptor CCR2 (CCR2$^+$ HSPCs). After myocardial ischemic injury or exposure to bacterial lipopolysaccharide (LPS), CCR2$^-$ HSCs remain quiescent while CCR2$^+$ HSPCs replicate robustly. These observations identify the hematopoietic

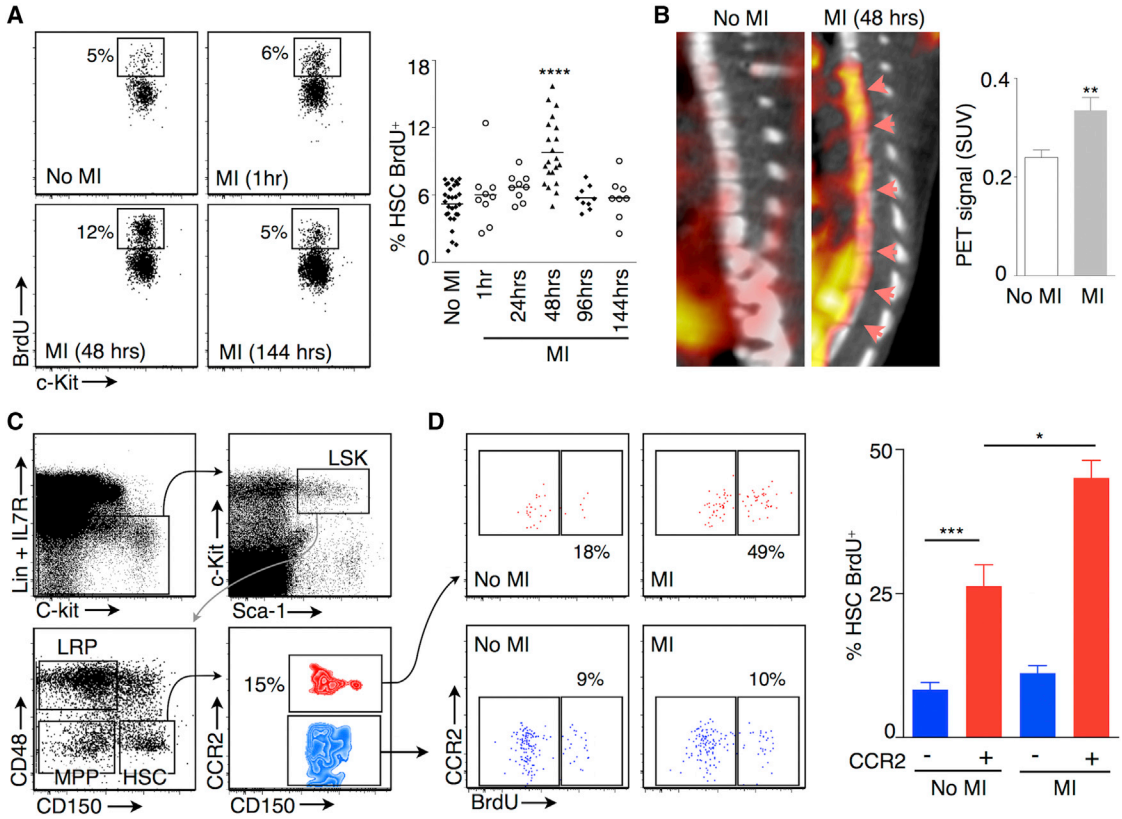

Figure 1. Activation of HSPCs after MI

(A) CD48$^-$CD150$^+$ HSC proliferation measured by BrdU incorporation with flow cytometry in steady state (No MI) and at different time points after MI (permanent coronary ligation, n = 8–29 per group). Hours refer to the time of BrdU injection after coronary ligation.

(B) Proliferation imaged by ^{18}F-FLT-PET/CT in bone marrow 2 days after MI. Arrow heads indicate increased PET signal in the vertebral marrow (n = 5–6 per group).

(C) Flow cytometric gating strategy for CCR2$^+$CD150$^+$CD48$^-$ LSKs, LRPs, and MPPs.

(D) Proliferation of CD48$^-$CD150$^+$CCR2$^+$ and CCR2$^-$ LSKs in steady state and 48 hr after MI (n = 5–17 per group) in mice. Data are shown as mean ± SEM, *p < 0.05, **p < 0.01, ***p < 0.001, ****p < 0.0001. See also Figure S1.

system's point of activation during severe stress and provide new insight into the pathogenesis of a highly prevalent disease.

RESULTS

MI Triggers Myelopoiesis in the Bone Marrow by Activating CCR2$^+$ HSPCs

MI results in leukocytosis and massive infiltration of myeloid cells into the injured heart (Swirski and Nahrendorf, 2013). Since myeloid cells in the infarct turn over in <24 hr (Leuschner et al., 2012), the high demand must be met by hematopoietic organs, and new cells arise from hematopoietic stem and progenitor cells (HSPCs). By following the bone marrow hematopoietic lineage upstream, we found increased proliferation of even the most primitive progenitor cells in mice with coronary ligation. In the femur, CD150$^+$CD48$^-$ HSCs (Figure 1A) and Lineage$^-$Sca-1$^+$c-Kit$^+$ cells (LSKs) (Figure S1A) incorporate the highest levels of the proliferation marker BrdU 48 hr after MI. Because BrdU may be mitogenic (Takizawa et al., 2011), we confirmed this proliferation peak with cell-cycle analysis on day 2 after coronary ligation while comparing to controls without ischemia. After MI, the percentage of quiescent HSCs and LSKs in G0 phase decreases while more HSCs and LSKs proliferate (G1 and S-G2-M phases) (Figures S1B and S1C). This results in more numerous HSCs, LSKs, multipotent progenitor cells (MPPs), and lineage-restricted progenitors (LRPs) in the femur bone marrow on day 3 after MI (Figure S1D). ^{18}F-FLT-PET/CT, a clinical imaging method for measuring cellular proliferation in cancer (Shields et al., 1998), detected increased signal in mouse vertebrae, indicating that MI induces widespread bone marrow response (Figure 1B) and that imaging may be used to monitor hematopoiesis.

While the vast majority of HSCs are quiescent, we hypothesized—in line with recent reports on HSC heterogeneity in the steady state (Mossadegh-Keller et al., 2013; Oguro et al., 2013)—that MI activates a specific HSC subset. Newly made monocytes rely on the chemokine receptor CCR2 for their departure from the bone marrow (Serbina and Pamer, 2006) and recruitment to the infarct (Dewald et al., 2005). CCR2 also identifies certain cardiac macrophage subsets (Epelman et al., 2014) and guides HSPCs to the inflamed peritoneum (Si et al., 2010). We hypothesized that a CCR2$^+$ HSPC subset might give rise to the systemic increase in CCR2$^+$ leukocytes during MI. Indeed,

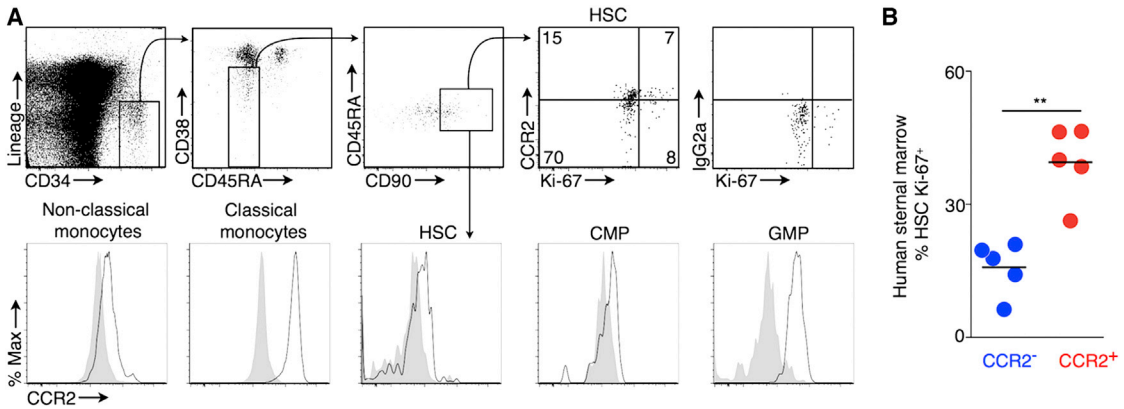

Figure 2. Human CCR2$^+$ Expression in HSCs

(A) CCR2 expression on both human non-classical monocytes and classical monocytes in the blood and CMPs, GMPs, and HSCs in the bone marrow harvested from the sternum during open heart surgery. The gating strategy for human HSCs is shown. The uppermost right panel shows isotype control staining for the CCR2 antibody.

(B) Proliferation of human CCR2$^+$ and CCR2$^-$ HSPCs (n = 5 per group).

Data are shown as mean ± SEM, **p < 0.01. Patient characteristics are listed in Table S1.

about 15% of CD48$^-$CD150$^+$ HSCs express CCR2 at high levels (Figure 1C). To test the specificity of FACS staining for CCR2, we examined HSCs in CCR2$^{+/RFP}$ mice, in which we detected a similar RFP$^+$ HSC frequency of 15% (Figure S1E). CCR2$^+$ CD150$^+$CD48$^-$ LSKs also contain higher levels of CCR2 mRNA when compared to their CCR2$^-$ counterparts (Figure S1E).

CCR2$^+$ HSPCs proliferate significantly more than CCR2$^-$ HSCs in steady state, as assessed by BrdU incorporation (Figure 1D) and BrdU-independent cell-cycle analysis (Figure S1F). 48 hr after coronary ligation, the gap in proliferative activity widens in these subsets; the fraction of BrdU$^+$CCR2$^+$ CD150$^+$CD48$^-$ LSKs increases to >40% whereas the fraction of BrdU$^+$CCR2$^-$ CD150$^+$CD48$^-$ LSKs remains at low levels (Figure 1D). However, HSC proliferation in *CCR2*$^{-/-}$ mice was similar to that in wild-type mice (Figure S1G). Analysis of human HSCs harvested from the sternal bone marrow of patients (Table S1) undergoing median sternotomy for open heart surgery confirmed CCR2 expression by an HSC subset (Figure 2A) and the higher proliferation of CCR2$^+$CD150$^+$CD48$^-$ LSKs (Figure 2B) observed in mice.

Electron microscopy revealed that murine CCR2$^+$CD150$^+$ CD48$^-$ LSKs aggregate ribosomes (Figure 3A), indicating active protein synthesis (Hardesty et al., 1963) in association with increased cell proliferation. Depending on their proliferative activity, HSPCs may reside in different bone marrow regions, with more primitive and quiescent cells locating to the vicinity of bone (Lo Celso et al., 2009; Nombela-Arrieta et al., 2013; Morrison and Scadden, 2014). Intravital microscopy after co-transfer of CCR2$^-$ and CCR2$^+$CD150$^+$CD48$^-$ LSKs labeled with spectrally distinct fluorescent membrane dyes mapped the cells' distribution in the skull calvarium bone marrow. Matching their state of quiescence and activity, the majority of CCR2$^-$ HSCs reside near the endosteum, whereas CCR2$^+$ HSPCs are more distant (Figure 3B). We next examined similarities and differences between CCR2$^+$ and CCR2$^-$CD150$^+$CD48$^-$ LSKs sorted from steady-state mouse bone marrow using Affymetrix microarrays. In a transcriptome-wide unsupervised hierarchical clustering analysis, CCR2$^+$ and CCR2$^-$CD150$^+$CD48$^-$ LSKs clearly segregated, pointing to global differences in their gene expression programs (Figure 3C and Table S2). Because rescue capacity distinguishes HSCs from hematopoietic progenitor cells, we investigated if CCR2$^+$CD150$^+$CD48$^-$ LSKs can rescue lethally irradiated mice. To this end, we injected lethally irradiated mice with either 100 CCR2$^-$ or 100 CCR2$^+$CD150$^+$CD48$^-$ LSK and Sca-1-depleted supportive bone marrow cells. CCR2$^-$ HSCs rescued seven out of eight mice, whereas CCR2$^+$ cells rescued six out of ten mice (Figure 3D). 120 days after the first transplantation, both CCR2$^-$ and CCR2$^+$CD150$^+$CD48$^-$ LSK reconstitution gave rise to multilineage chimerism, which was biased toward the myeloid lineage in mice that received CCR2$^+$ cells (Figure S2A). In a secondary host, which received either 100 CCR2$^-$ or CCR2$^+$CD150$^+$CD48$^-$ LSKs isolated from primary recipients, CCR2$^+$ cells exhausted their self-renewal capability while CCR2$^-$ HSCs did not (Figure S2B). In contrast to the primary host, CCR2$^+$CD150$^+$CD48$^-$ LSK-derived leukocyte chimerism was markedly reduced 5 weeks after secondary transplantation (Figure S2C). We used a limiting dilution assay to determine the number of functional HSCs within CCR2$^-$ or CCR2$^+$CD48$^-$CD150$^+$ LSKs harvested from steady-state bone marrow (Figure 3E). Irradiated recipients received dilutions between 31 to 1,000 cells isolated by flow cytometry. Four months later, less than 0.1% multilineage blood chimerism determined the non-responding fraction of recipient mice. The frequency of functional HSCs was 6.5-fold higher within CCR2$^-$ HSCs when compared to the CCR2$^+$ subset (Figure 3E). However, a second limiting dilution assay indicated that the frequency of functional HSCs is unchanged in *CCR2*$^{-/-}$ bone marrow (Figure S2D). All together, these data suggest that CCR2$^+$ HSPCs represent a functionally distinct subset with reduced self-renewal capacity in secondary hosts, and that this HSPC subset undergoes preferential activation during MI. The data further implicate that CCR2 may serve as a marker to identify this actively proliferating HSPC subset in mice and humans. However, genetic deficiency of CCR2 alters neither HSC proliferation nor frequency.

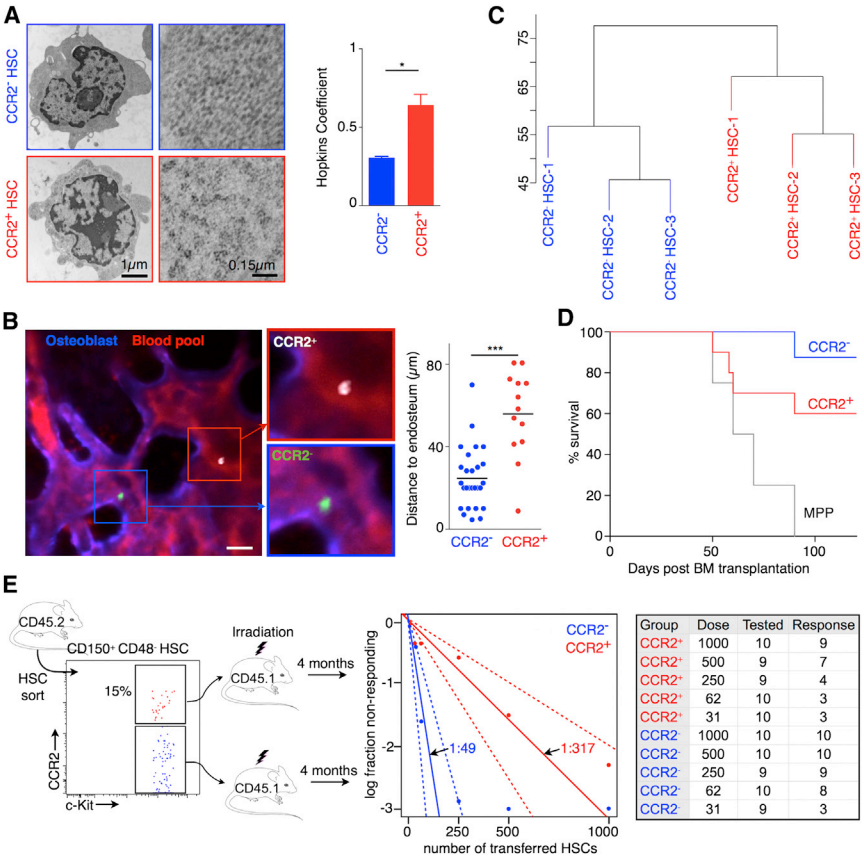

Group	Dose	Tested	Response
CCR2⁺	1000	10	9
CCR2⁺	500	9	7
CCR2⁺	250	9	4
CCR2⁺	62	10	3
CCR2⁺	31	10	3
CCR2⁻	1000	10	10
CCR2⁻	500	10	10
CCR2⁻	250	9	9
CCR2⁻	62	10	8
CCR2⁻	31	9	3

Figure 3. CCR2⁺ HSPC Phenotype, Location, and Function

(A) Electron microscopy images of cell subsets (left panel) and magnified cytosol showing distribution of ribosomes (right panel). The bar graph shows ribosome aggregation in subsets (one-tail Wilcoxon rank sum test, p = 0.036) (n = 6 ROIs in three CCR2⁺ and n = 13 ROIs in five CCR2⁻ HSPCs).

(B) DiO-labeled CCR2⁻ and DiD-labeled CCR2⁺ CD150⁺CD48⁻ LSKs were imaged in the skull with intravital microscopy 1 day after transfer (n = 13–27 cells in two mice per group). DiO-labeled CCR2⁻ HSCs are green, DiD-labeled CCR2⁺ HSPCs are white, blood pool is red, and osteoblasts are blue. The scale bar represents 20 μm.

(C) Hierarchical clustering dendrogram based on whole-transcriptome microarray data of CCR2⁺ and CCR2⁻CD150⁺CD48⁻ LSKs sorted from steady-state bone marrow (three replicates per group).

(D) Survival curve of lethally irradiated mice reconstituted with CCR2⁻ (n = 8), CCR2⁺ (n = 10), CD150⁺CD48⁻ LSKs, or MPPs (n = 4).

(E) Limiting dilution assay determined functional HSC frequency among CCR2⁻ and CCR2⁺ CD150⁺CD48⁻ LSKs in wild-type bone marrow. Multilineage blood chimerism of 0.1% or higher served as a cut-off value to determine responders ($p < 0.001$ for difference in frequency). Table lists dilution steps, numbers of mice analyzed 4 months after HSC transfer, and number of responders.

Data are shown as mean ± SEM, *p < 0.05, ***p < 0.001. See also Figure S2 and Table S2.

Myeloid Translocation Gene on Chromosome 16 Activity in CCR2⁺ HSPCs

To understand the molecular mechanisms underlying the distinct functions of CCR2⁺CD150⁺CD48⁻ LSKs, we contrasted their gene expression profiles with CCR2⁻CD150⁺CD48⁻ LSKs using gene set enrichment analysis. Of 78 gene sets that were upregulated in CCR2⁺ HSPCs at a 25% false discovery rate (FDR) cutoff, the most significant set contained genes regulated by myeloid translocation gene on chromosome 16 (*Mtg16*), a transcriptional co-repressor required for hematopoietic progenitor cell fate decisions and early progenitor cell proliferation (Chyla et al., 2008). Specifically, genes previously found downregulated in *Mtg16*$^{-/-}$ mouse bone marrow progenitor cells were enriched in CCR2⁺ HSPCs, while genes upregulated upon *Mtg16* knockout were enriched in CCR2⁻ HSCs (ranked as fourth significant among 1,222 gene sets with an FDR < 25%) (Figure 4A). We performed qPCR to determine any difference in the subsets' expression of *Mtg16* or the transcription factors to which it binds (Hofmann et al., 2002; Okuda et al., 2001; Semerad et al., 2009; Summers et al., 2013; Young et al., 2004). CCR2⁺ HSPCs express significantly higher levels of Mtg16 than CCR2⁻ HSCs (Figure 4B). Of the regulatory factors, Prkar2a, which increases in HSCs of patients with myelodysplastic syndrome (Hofmann et al., 2002), was higher in CCR2⁺ HSPCs (Figure S3A). *Mtg16*$^{-/-}$ mice have fewer CCR2⁺ HSPCs while CCR2⁻ HSC levels appear unchanged (Figure 4C). The paucity of CCR2⁺ HSPCs in *Mtg16*$^{-/-}$ mice associates with decreased HSC proliferation after MI (Figures S3B and S3C) and fewer monocytes and macrophages in the blood (Figure 4D) and infarct tissue (Figure 4E) on day 3 after coronary ligation. In line with this observation, *Mtg16* expression was higher in HSCs during the active S-G2-M phases of the cell cycle in steady state (Figure S3D) and after a 5FU challenge (Figures S3E–S3G), indicating an association of *Mtg16* and cell proliferation. Of note, proliferating CCR2-deficient HSCs are still able to increase *Mtg16* expression after MI, demonstrating that CCR2 does not regulate *Mtg16* expression (Figure S3H). To evaluate the relative contribution to myelopoiesis after MI, we injected GFP⁺ CCR2⁻ or CCR2⁺CD150⁺CD48⁻ LSKs into CD45.1 mice on day 4 after coronary ligation. Four days after transfer, we investigated the progeny of transferred cells in the recipient's blood and infarcts (Figure 4F). We found significantly higher numbers of leukocytes produced by CCR2⁺CD150⁺CD48⁻ LSKs when compared to progeny of transferred CCR2⁻CD150⁺CD48⁻ LSKs. Almost all infarct leukocytes derived from CCR2⁺ HSPCs were myeloid cells (Figure 3F). These data indicate that CCR2⁺ HSPCs contribute to the infarct myeloid cell population; however, the functional implications for recovery after MI were still unclear. To explore this question, we investigated infarct healing in *Mtg16*$^{-/-}$ mice with severely reduced CCR2⁺CD150⁺CD48⁻ LSKs. Seven days after coronary ligation, protease activity, which is tightly linked to myeloid cell function, was lower in infarcts of *Mtg16*$^{-/-}$ mice (Figure 4G). Serial cardiac MRI reported a comparable infarct size on day 1 after coronary ligation in wild-type and *Mtg16*$^{-/-}$ mice (Figure S3I), but left ventricular dilation accelerated in *Mtg16*$^{-/-}$ mice (Figure 4H). In parallel, immunoreactive staining for the macrophage surface marker CD68, myofibroblasts, and collagen-1

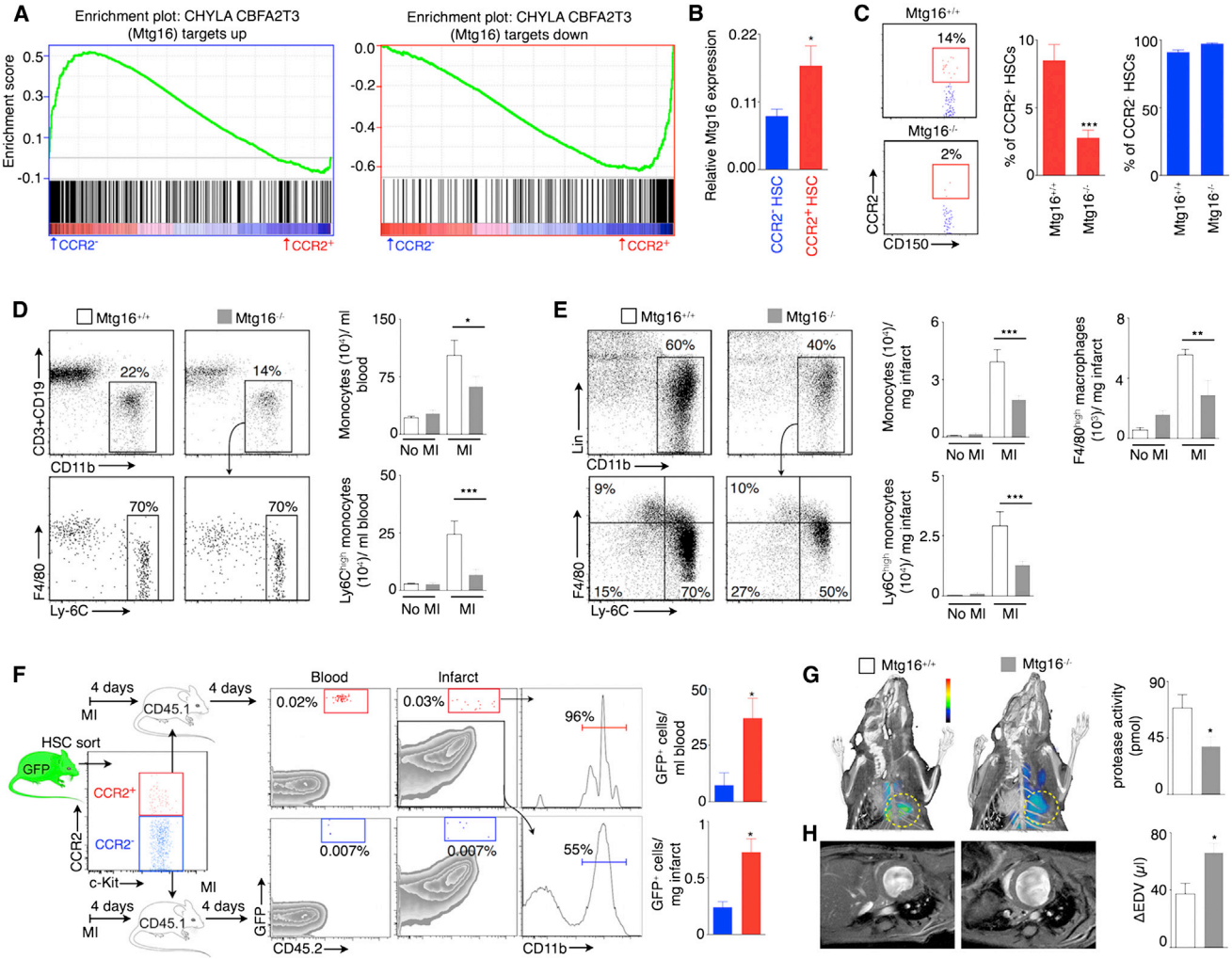

Figure 4. Role of Mtg16 in Myelopoiesis

(A) Gene set enrichment analysis showing that CCR2$^+$ HSPCs express genes that are downregulated in hematopoietic stem and progenitor cells in *Mtg16*$^{-/-}$ mice, while CCR2$^-$ HSCs express genes that are upregulated in *Mtg16*$^{-/-}$ (FDR q < 0.001 in both cases).

(B) *Mtg16* mRNA expression in HSCs normalized to Gapdh (n = 6 per group).

(C) Percentage of CCR2$^+$ and CCR2$^-$CD150$^+$CD48$^-$ LSKs in wild-type and *Mtg16*$^{-/-}$ mice in steady state (n = 7–8 per group).

(D and E) FACS quantification of myeloid cells 3 days after MI in the blood (D) and infarct (E) of wild-type and *Mtg16*$^{-/-}$ mice (n = 4–6 per group).

(F) Seven thousand CCR2$^+$ or CCR2$^-$CD150$^+$CD48$^-$ LSKs were sorted from GFP$^+$ bone marrow and adoptively transferred into CD45.1 C57B/6 on day 4 after MI. Four days after transfer, progeny of GFP$^+$ cells were analyzed in the blood and infarct (n = 4 per group).

(G) In vivo protease imaging in wild-type and *Mtg16*$^{-/-}$ mice on day 7 after MI (infarct indicated by yellow circle) (n = 10–12 per group).

(H) Change in end-diastolic volume (Δ EDV) between day 1 and 21 after MI in wild-type and *Mtg16*$^{-/-}$ mice measured with cardiac MRI. Original MR images show representative end-diastolic mid-ventricular short axis view 21 days after MI (n = 6–7 per group).

Data are shown as mean ± SEM, *p < 0.05, **p < 0.01, ***p < 0.001. See also Figure S3.

decreased 7 days after coronary ligation in infarcts of *Mtg16*$^{-/-}$ mice (Figure S3J). Taken together, these data link an insufficient number of CCR2$^+$ HSPCs with decreased macrophage supply to the ischemic wound, which impaired infarct healing and recovery after ischemic organ injury.

Hierarchy and Lineage Bias

Gene set enrichment analysis indicated that CCR2$^-$ HSCs express genes associated with upstream HSCs (ranked 19th among 1,222 significant gene sets) (Figure 5A), thereby suggesting these cells hold a higher hierarchical position. Principal components analysis of the whole transcriptome corroborates this observation: CCR2$^-$ HSCs are in proximity to upstream CD34$^-$ LSKs while CCR2$^+$ HSPCs distribute closer to myeloid cells (Figure 5B). To test directly the subset's lineage relationships, we co-transferred CD45.2 CCR2$^-$ and CD45.1 CCR2$^+$CD150$^+$CD48$^-$ LSKs into lethally irradiated mice and investigated reconstitution 4 months later. CCR2$^-$ HSCs have a higher reconstitution capability and can generate CCR2$^+$ HSPCs (Figure 5C). CCR2$^+$ CD150$^+$CD48$^-$ LSKs failed to give rise to CCR2$^-$ CD150$^+$CD48$^-$ LSKs, confirming that CCR2$^-$ HSCs are more primitive (Figure 5C). Since HSCs harvested from CD45.2$^+$ mice engraft better

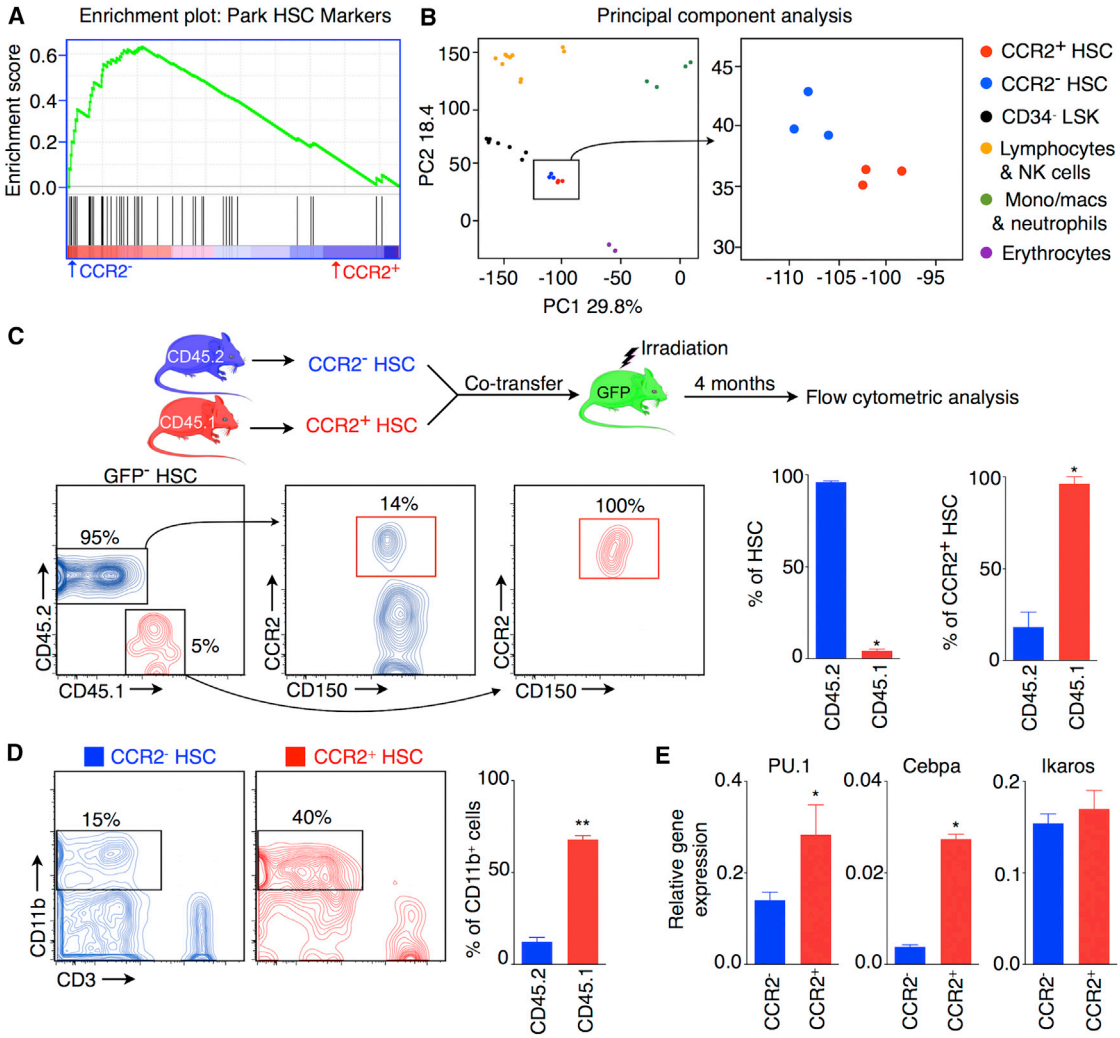

Figure 5. Lineage Relationship between CCR2$^+$ and CCR2$^-$CD150$^+$CD48$^-$ LSKs

(A) Gene set enrichment analysis for HSC genes shows enrichment in CCR2$^-$ HSCs (FDR q = 0.001).

(B) Principal components analysis. Projection of CCR2$^+$ and CCR2$^-$CD48$^-$CD150$^+$ LSKs into the same space as mouse HSCs, leukocytes, and erythrocytes shows differentiation of CCR2$^+$CD150$^+$CD48$^-$ LSKs along the myeloid lineage.

(C) Upper panel: Experimental design for competitive bone marrow reconstitution with 100 CCR2$^+$ and CCR2$^-$CD150$^+$CD48$^-$ LSKs. Lower panel: plots showing HSC chimerism in the bone marrow and percentage of CCR2$^+$CD150$^+$CD48$^-$ LSKs derived from transferred cells. The bar graphs depict quantified flow cytometric data (n = 4 per group).

(D) Blood chimerism in myeloid cells derived from transferred HSCs 4.5 months after bone marrow reconstitution (n = 3 per group).

(E) mRNA levels of myeloid (PU.1 and Cebpa) and lymphoid (Ikaros) transcription factors in FACS-isolated CCR2$^+$ and CCR2$^-$CD150$^+$CD48$^-$ LSKs, normalized to Gapdh (n = 3–10 per group).

Data are shown as mean ± SEM, *p < 0.05, **p < 0.01. See also Figure S4.

than CD45.1 HSCs (Purton and Scadden, 2007), we switched the HSC subtype's sources; however, CCR2$^-$ HSCs still reconstituted better (data not shown). Slamf3 (CD229)$^-$ and Slamf4 (CD244)$^-$ HSCs were previously classified as quiescent HSCs (Oguro et al., 2013), and our observation that CCR2$^-$ HSCs contain higher percentages of Slamf3$^-$ and Slamf4$^-$ cells (Figure S4A) supports that classification. In contrast to most MPPs (Yang et al., 2005), CCR2$^+$ HSPCs do not express FLK-2 (Figure S4B), which, together with expression of the SLAM family markers and long-term multilineage repopulation capacity in lethally irradiated mice, distinguishes CCR2$^+$ HSPCs from downstream MPPs on phenotypic and functional levels. After reconstituting irradiated recipients, CCR2$^+$ HSPCs give rise to a higher percentage of CD11b$^+$ cells, which indicates their myeloid bias (Figure 5D and Figures S4C–S4E). Consistent with this finding, CCR2$^+$ HSPCs express higher levels of the transcription factors PU.1 and Cebpa (Figure 5E). In contrast, CCR2$^-$ and CCR2$^+$ CD150$^+$CD48$^-$ LSKs comparably express Ikaros, a lymphoid transcription factor (Figure 5E).

During MI Bone Marrow Preferentially Releases CCR2$^+$ HSCs

CCR2 is involved in monocyte (Charo and Peters, 2003) and progenitor cell (Si et al., 2010) migration. Accordingly, genes

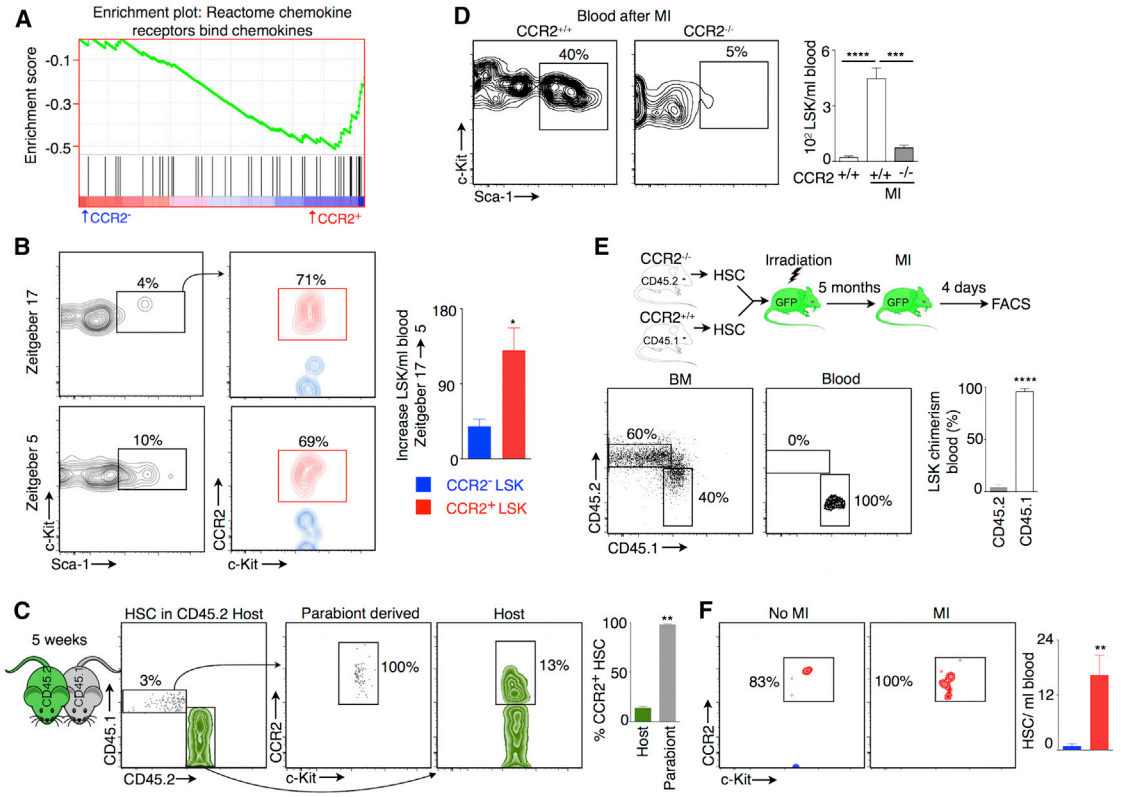

Figure 6. Migration of CCR2⁺CD150⁺CD48⁻ LSKs from the Bone Marrow in Steady State and after MI

(A) Gene set enrichment analysis for chemokines and chemokine receptors shows enrichment in CCR2⁺CD150⁺CD48⁻ LSKs (FDR q < 0.05).

(B) Percentage of CCR2⁺ and CCR2⁻CD150⁺CD48⁻ LSKs in the blood during steady state at Zeitgeber 17 (midnight) and Zeitgeber 5 (noon) (n = 4 per group).

(C) CD45.1 and CD45.2 mice were analyzed after 5 weeks of parabiosis. Only CCR2⁺CD150⁺CD48⁻ LSKs migrated to the other bone marrow of the other parabiont. The plots and the bar graph depict the percentage of CCR2⁺ host and migratory CD150⁺CD48⁻ LSKs in the bone marrow (n = 5 per group).

(D) LSKs in blood in *CCR2*$^{-/-}$ and wild-type mice 4 days after the inducement of myocardial infarction (MI) (n = 5–12 per group).

(E) Upper panel: experimental design to investigate CCR2-dependent emigration from the bone marrow after MI. Lower panel: percentage of LSK chimerism in the blood (normalized to bone marrow chimera) 4 days after MI (n = 5 per group).

(F) Post-MI HSC release into blood is dominated by CCR2⁺CD150⁺CD48⁻ LSKs. FACS plots are gated on HSCs. The bar graph depicts the increase of absolute HSC numbers in blood from steady state to day 3 after MI (n = 8–9 per group). Data are shown as mean ± SEM, *p < 0.05, **p < 0.01, ***p < 0.001, ****p < 0.0001. See also Figure S5.

associated with cellular migration are enriched in CCR2⁺ CD150⁺CD48⁻ LSKs (ranked ninth out of 78 significant gene sets) (Figure 6A). Even though only 15% of bone marrow HSCs express CCR2, most (>90%) LSKs and HSCs in the blood and spleen are CCR2⁺ (Figure S5A). HSCs release from the bone marrow following circadian oscillations (Méndez-Ferrer et al., 2008) (Figure 6B), with a migration peak at noon (Zeitgeber 5). We found that the majority of LSKs released in steady-state circadian oscillation express CCR2 at high levels (Figure 6B). To investigate HSC migration during steady state, we put CD45.2 and CD45.1 mice into parabiosis (Figure 6C and Figure S5B). After 5 weeks of joint circulation, we evaluated the expression of CCR2 on HSCs that had migrated from one mouse to the bone marrow of the other. All CD45.1⁺ parabiont-derived HSCs in the bone marrow of CD45.2 mice expressed CCR2 at high levels (Figure 6C). Together, these data indicate that only CCR2⁺ CD150⁺CD48⁻ LSKs have migratory capacity in the steady state and confirm our adoptive transfer data (Figure 5C) showing that CCR2⁺ cells do not revert to CCR2⁻ HSCs.

Post-MI HSPC release from the bone marrow enables extramedullary amplification of myelopoiesis and exacerbates inflammation in atherosclerotic plaque due to outsourced and accelerated splenic leukocyte production (Robbins et al., 2012; Leuschner et al., 2012; Dutta et al., 2012). Because we found that most migrating HSCs are CCR2⁺ during steady state, we tested whether infarct-induced HSC release also depends on CCR2. We induced MI in *CCR2*$^{-/-}$ mice and found impaired LSK release into blood (Figure 6D and Figure S5C). Knocking down CCR2 in HSCs with lipidoid nanoparticle-delivered siRNA (Leuschner et al., 2011) reduces the MI-induced LSK release (Figures S5D–S5F) and consecutive splenic seeding (Figure S5G). In fact, siRNA may be an avenue for therapeutic intervention aiming to reduce the production and supply of inflammatory leukocytes. To investigate further if *CCR2*$^{-/-}$ LSKs can leave the bone marrow, we generated mixed bone marrow chimeras by reconstituting lethally irradiated GFP⁺ mice with both *CCR2*$^{-/-}$ and *CCR2*$^{+/+}$ HSCs (Figure 6E). Upon induction of MI, only *CCR2*$^{+/+}$ LSKs leave the bone marrow (Figure 6E).

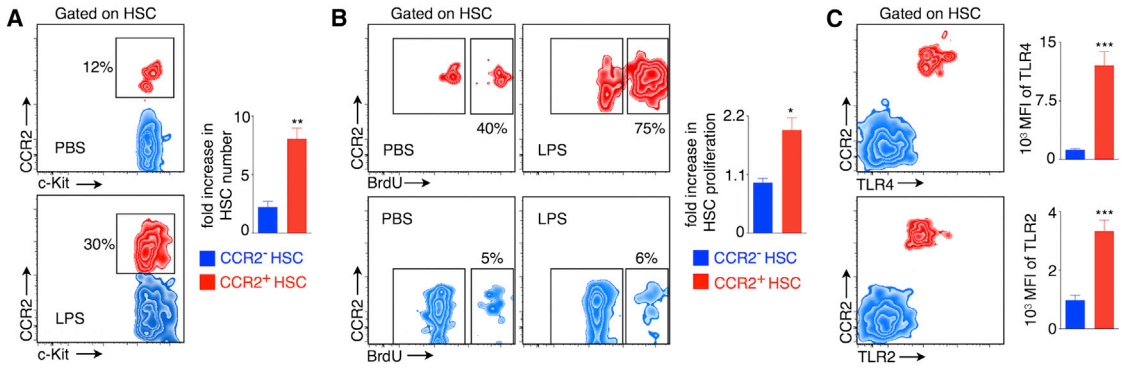

Figure 7. CCR2⁺ HSPCs after LPS Treatment

(A) Fold change of CCR2⁺ and CCR2⁻CD150⁺CD48⁻ LSK number in bone marrow of LPS-injected mice compared to PBS-injected controls at 4 hr after injection (n = 4 per group).

(B) Fold change of proliferation 4 hr after injection of LPS (n = 6 per group).

(C) Steady state TLR4 and TLR2 expression levels on HSCs (n = 9 per group).

Data are shown as mean ± SEM, *p < 0.05, **p < 0.01, ***p < 0.001. See also Figure S6.

In wild-type mice, the increase of circulating HSPCs on day 3 after MI relies exclusively on CCR2⁺CD150⁺CD48⁻ LSKs (Figure 6F). To investigate if stromal bone marrow cells produce more CCL2 after MI, we isolated endothelial and mesenchymal stem cells from the bone marrow on day 4 after coronary ligation, as both are potential sources for the chemokine (Shi et al., 2011). After MI, only endothelial cells express elevated levels of CCL2 mRNA (Figure S5H), indicating that CCL2 produced by endothelial cells could mobilize CCR2⁺ HSPCs from their niche.

CCR2⁺ HSPCs Are Activated after LPS and HMGB1 Challenge

Finally, we wondered if the role of CCR2⁺ HSPCs is specific to MI or whether this cell subset has broader functions. Thus, we challenged mice with LPS, an endotoxin contained in the cell walls of Gram-negative bacteria. CCR2⁺ HSPCs expanded in the bone marrow 4 hr after injection of this Toll-like receptor ligand (Figure 7A). Measuring BrdU incorporation, we found that only CCR2⁺ HSPCs increase proliferation after LPS challenge (Figure 7B). Preferential activation of CCR2⁺ HSPCs at 4 hr after LPS injection suggests that this subset expresses high levels of receptors that sense danger-associated molecular patterns (DAMPs). Accordingly, CCR2⁺ CD150⁺CD48⁻ LSKs express significantly higher levels of TLR4 and TLR2 when compared to CCR2⁻ CD150⁺CD48⁻ LSKs (Figure 7C). In the context of cardiovascular disease, ischemic injury may release DAMPs that ligate TLRs. Indeed, CCR2⁺ HSPCs increase TLR4 expression after MI (Figure S6A). Injection of HMGB1, which is released by cardiomyocytes during acute MI (Arslan et al., 2011), enhances CCR2⁺ HSPC proliferation (Figure S6B).

DISCUSSION

The white blood count is one of the most frequently ordered medical tests, reflecting its clinical value. In cardiovascular patients, leukocytosis and monocytosis closely correlate with survival. We increasingly understand why: inflammatory monocytes and macrophages, when overproduced, damage the arterial wall and vital organs such as the heart after MI or the brain after stroke. We have surprisingly limited understanding of mechanisms leading to increased leukocyte count in cardiovascular patients. Chronic leukocytosis affiliated with hyperlipidemia arises from perturbed cholesterol efflux, which makes hematopoietic progenitors cycle more vigorously (Yvan-Charvet et al., 2010) and gives rise to progressively elevated monocyte counts in mice with atherosclerosis (Swirski et al., 2006; Tacke et al., 2007). MI induces enhanced extramedullary myelopoiesis due to increased progenitor cell traffic between the marrow and the spleen (Dutta et al., 2012). Even though insufficient and exuberant leukocyte production after MI associates with poorer prognosis (Nahrendorf et al., 2010), the mechanisms that link ischemic injury to changes in hematopoiesis at the stem cell level have remained obscure.

This study identifies preferential activation of a CCR2⁺CD150⁺ CD48⁻ LSK subset during MI or exposure to a bacterial danger signal, LPS. In contrast, CCR2⁻CD150⁺CD48⁻ LSKs remain quiescent in stress conditions. Thus, CCR2⁺CD48⁻CD150⁺ LSKs represent the most upstream point of increased myelopoiesis after MI. In contrast to retrospectively identifiable myeloid-restricted progenitors with long-term repopulation activity (Yamamoto et al., 2013), CCR2 serves as a cell surface marker to prospectively identify a highly active cell population within the CD150⁺CD48⁻ SLAM HSC gate. CCR2 also participates functionally by mediating migratory cell activity during MI. A few HSPCs migrate even in the steady state, possibly to survey peripheral organs (Massberg et al., 2007). Of direct relevance to the present observations, CCR2⁺ cells dominate in this migratory population. Moreover, CCR2⁺ HSPCs express receptors of DAMPs such as TLR4 and TLR2. They increase expression of these receptors further after MI, rendering them sensitive to danger signals, such as HMGB1, released from the dead myocardium. In addition, CCR2⁺CD150⁺CD48⁻ LSKs are also preferentially activated after LPS challenge.

After MI, activity of the sympathetic nervous system triggers bone marrow release of HSPCs into circulation in larger numbers, thus enabling the outsourcing of inflammatory cell production to the spleen (Dutta et al., 2012). Splenic myelopoiesis replenishes the organ's monocyte reservoir, which supplies cells in the first 24 hr after injury (Swirski et al., 2009) but also supports

continued contribution of cells to the heart (Leuschner et al., 2012). In healing infarcts and other wounds, the initial need for macrophages is followed by the necessity for resolution of inflammation. The observation of impaired infarct healing in *Mtg16*$^{-/-}$ mice with an insufficient supply of infarct macrophages underscores the cell's contribution to tissue repair. However, if inflammation resolution is delayed, infarcts rupture and heart failure occurs. Thus, the supply of inflammatory cells, which are initially important for clearing dead cells and the orchestration of tissue repair, should wind down as wound healing progresses to proliferative stages. The post-MI bone marrow release of CCR2^{+}CD150^{+}CD48^{-} LSKs, which excel at migration and myeloid cell production but have a lower self-renewal capacity than CCR2^{-}CD150^{+}CD48^{-} LSKs, may hypothetically amount to a program of expanded leukocyte production with a built-in exit strategy. If likewise released, CCR2^{-} HSCs would ignite indefinite extramedullary hematopoiesis and thus perpetuate systemic inflammation, a complication that is likely avoided by limiting bone marrow cell exit to CCR2^{+} HSPCs that exhaust in secondary transplantation assays.

Since CCR2^{+}CD150^{+}CD48^{-} LSKs do not rescue secondary hosts, they are not long-term HSCs. CCR2^{+}CD150^{+}CD48^{-} LSKs share phenotypic markers with short-term HSCs, as they express CD34, but not FLK-2, and resemble short-term HSCs in their failure to repopulate secondary hosts (Yang et al., 2005). CCR2^{+}CD150^{+}CD48^{-} LSKs generate multilineage chimerism in primary recipients 4 months after reconstitution and rescue lethally irradiated primary hosts, which places them functionally above short-term HSCs according to some definitions (Reya et al., 2001; Challen et al., 2009); however, they resemble recently described upstream MPP-1 (Cabezas-Wallscheid et al., 2014). We therefore refer to these cells as "CCR2^{+} HSPCs."

Unchanged functional HSC frequency and proliferation in *CCR2*$^{-/-}$ mice indicates that CCR2 does not regulate stem cell replication after MI. Rather, we identify Mtg16 as a molecular decision node in HSPCs and, consecutively, in monocyte production. The dampened post-MI myelopoiesis and compromised infarct healing in *Mtg16*$^{-/-}$ mice may be caused by the lack of the CCR2^{+} HSPC subset but could additionally reflect compromised responses of downstream progenitors. Despite growing evidence of inflammation's importance in ischemic heart disease, specific anti-inflammatory therapeutic approaches have only begun to emerge. The data presented here indicate that targeting CCR2^{+} HSPCs, for instance via CCR2 or Mtg16, might reduce emergency monocyte production, curb macrophage oversupply, and limit excessive tissue destruction during acute inflammation triggered by ischemic injury.

EXPERIMENTAL PROCEDURES

Animal Models and Surgeries

All mouse studies were approved by the Subcommittee on Animal Research Care at Massachusetts General Hospital. C57BL/6J, C57BL/6-Tg(UBC-GFP)30Scha/J, B6.SJL-Ptprc^{a} Pepc^{b}/BoyJ (CD45.1), B6.129S4-*Ccr2*^{tm1fc}/J (*CCR2*$^{-/-}$), and B6.129(Cg)-Ccr2$^{tm2.1Ifc}$/J (CCR2$^{+/RFP}$) mice were purchased from Jackson Laboratory. For all experiments, 4- to 5-month-old mice were used. To induce MI, thoracotomy in the fourth left intercostal space was performed after intubation and ventilation with 2% isoflurane. The left coronary artery was permanently ligated with a monofilament nylon 8-0 suture, and the thorax was closed with a 5-0 suture. For parabiosis, an incision was made on the skin on the lateral sides of mice starting from the ear reaching the tail. Corresponding scapulae were joined using a 6-0 suture. A 0.5 cm incision was made on the abdomen and approximated with a 6-0 suture. The skin was sutured with mono-nylon 6-0 (Ethicon).

Flow Cytometry

Cells diluted in 300 μl of FACS buffer were stained with fluorochrome-labeled antibodies against mouse leukocyte markers and hematopoietic stem and progenitor cell markers. For leukocyte staining, a phycoerythrin (PE) lineage cocktail was used, which contains antibodies directed against CD90 (clone 53-2.1), B220 (clone RA3-6B2), CD49b (clone DX5), NK1.1 (clone PK136), Ly-6G (clone 1A8), and Ter-119 (clone TER-119). Leukocytes were stained with anti-mouse CD11b (clone M1/70), CD11c (clone HL3), F4/80 (clone BM8) and Ly6C (clone AL-21). Monocytes were identified as (CD90/B220/ CD49b/NK1.1/Ly-6G/Ter119)^{low} CD11b^{high} F4/80^{low} CD11c$^{neg/low}$ Ly-6C$^{high/low}$. For stem and progenitor cell staining, we used biotin-conjugated antibodies against CD11b (clone M1/70), CD11c (clone N418), and IL7Rα (clone A7R34) in addition to the lineage antibodies used for leukocyte staining. The cells were then stained with anti c-Kit (clone 2B8), Sca-1 (clone D7), CD16/32 (clone 2.4G2), CD34 (clone RAM34), CD115 (clone AFS98), CD150 (9D1), CD48 (HM48-1), and CCR2 (RandD Biosystems clone: 475301; abcam: ab21667). HSCs were identified as lineage^{low} c-Kit^{high} Sca-1^{high} CD150^{+}CD48^{-}. Downstream progenitors such as LRPs and MPPs were identified as lineage^{low} c-Kit^{high} Sca-1^{high} CD150^{-}CD48^{+} and lineage^{low} c-Kit^{high} Sca-1^{high} CD150^{-} CD48^{-}, respectively.

Microarray Experiments and Data Analysis

For each sample, HSCs sorted from 20 B6 mice were pooled, and RNA was extracted as described above. cDNA was prepared using the Ovation Pico WTA System V2 (NuGEN) and hybridized to GeneChip® Mouse Gene 2.0 ST arrays (Affymetrix). Raw data were normalized using the robust multi-array average (Irizarry et al., 2003) and are available at GEO under accession number GEO: GSE53827. We eliminated probe sets with low variance across all samples (lower quartile) and performed hierarchical clustering using Euclidian distance and Ward's method. Differentially expressed genes were determined using Significance Analysis of Microarrays (Tusher et al., 2001). Probe sets with an FDR below 10% are provided in Table S1. We performed gene set enrichment analysis (Subramanian et al., 2005) with default parameters, except that we used class difference as a ranking metric and permuted gene sets instead of phenotype labels. To determine how the transcriptomes of CCR2^{+} and CCR2^{-}CD150^{+}CD48^{-} LSKs relate to gene expression in various other hematopoietic cells, we used a previously published method (Kho et al., 2004) based on principal components analysis to integrate our data with a reference dataset containing expression profiles of hematopoietic cells at different stages of differentiation (ranging from CD34^{-} HSCs to fully differentiated myeloid and lymphoid cells). Briefly, we obtained reference data from Konuma et al. (2011) (GEO: GSE27787) and collapsed both datasets to gene symbols, retaining only genes that were present on both arrays. We then performed a principal components analysis of the reference dataset and used the first two principal components to project both the Konuma data and our CCR2^{+} and CCR2^{-} gene expression profiles into a 2D space.

siRNA Treatment

siRNA (5-uGcuAAAcGucucuGcAAAdTsdT-3 [sense], 5-UUUGcAGAGACG UUuAGcAdTsdT-3 [anti-sense]) against CCR2 was formulated into lipid nanoparticles as described previously (Leuschner et al., 2011). B6 mice were injected intravenously with 0.5 mg/kg/day siRNA for 4 days after MI.

ACCESSION NUMBERS

The microarray data reported in this manuscript are available at GEO (http://www.ncbi.nlm.nih.gov/geo/) under accession number GEO: GSE53827.

SUPPLEMENTAL INFORMATION

Supplemental Information for this article includes six figures, two tables, and Supplemental Experimental Procedures and can be found with this article online at http://dx.doi.org/10.1016/j.stem.2015.04.008.

AUTHOR CONTRIBUTIONS

P.D. and H.B.S. designed and performed experiments, collected and analyzed the data, and contributed to writing the manuscript; K.R.S., K.N., G.C., B.S., L.S., T.H., M.S., G.W., P.F.F., K.K., J.N.B., A.v.d.L., A.B., K.F., Y.S., M.H., F.H., Y.I., C.V., D.B., M.D., and S.H. performed experiments, collected, analyzed, and discussed data. K.N., D.S., P.L., F.K.S., and R.W. conceived experiments and discussed strategy and results. M.N. designed and managed the study and contributed to writing the manuscript, which was edited and approved by all co-authors.

ACKNOWLEDGMENTS

We thank Michael Waring and Adam Chicoine from Ragon Institute (of MGH, MIT, and Harvard) and Laura Prickett-Rice, Kat Folz-Donahue, and Meredith Weglarz from the Flow Cytometry Core Facility (Massachusetts General Hospital, Center for Regenerative Medicine and Harvard Stem Cell Institute) for assistance with cell sorting. We also acknowledge Dr. Chee Lim, Vanderbilt Medical Center MMPC (supported by U24 DK059637) for help with infarct surgery. We thank Mary McKee (Program in Membrane Biology Microscopy) for help with electron microscopy. This work was funded in part by grants from the NIH: R01-HL096576, R01-HL117829, and R01-NS084863 (M.N.); HHSN268201000044C (R.W.); and K99-HL121076 (P.D.). Hendrik B. Sager and Timo Heidt were funded by Deutsche Forschungsgemeinschaft (SA1668/2-1 to H.B.S and HE-6382/1-1 to T.H.). Support for the Program in Membrane Biology Microscopy Core comes from the Boston Area Diabetes and Endocrinology Research Center (DK57521) and the MGH Center for the Study of Inflammatory Bowel Disease (DK43351). A.B. and K.F. are Alnylam Pharmaceuticals employees.

Received: April 30, 2014
Revised: February 2, 2015
Accepted: April 20, 2015
Published: May 7, 2015

REFERENCES

Arslan, F., de Kleijn, D.P., and Pasterkamp, G. (2011). Innate immune signaling in cardiac ischemia. Nat. Rev. Cardiol. *8*, 292–300.

Baldridge, M.T., King, K.Y., Boles, N.C., Weksberg, D.C., and Goodell, M.A. (2010). Quiescent haematopoietic stem cells are activated by IFN-gamma in response to chronic infection. Nature *465*, 793–797.

Cabezas-Wallscheid, N., Klimmeck, D., Hansson, J., Lipka, D.B., Reyes, A., Wang, Q., Weichenhan, D., Lier, A., von Paleske, L., Renders, S., et al. (2014). Identification of regulatory networks in HSCs and their immediate progeny via integrated proteome, transcriptome, and DNA Methylome analysis. Cell Stem Cell *15*, 507–522.

Challen, G.A., Boles, N., Lin, K.K., and Goodell, M.A. (2009). Mouse hematopoietic stem cell identification and analysis. Cytometry A *75*, 14–24.

Charo, I.F., and Peters, W. (2003). Chemokine receptor 2 (CCR2) in atherosclerosis, infectious diseases, and regulation of T-cell polarization. Microcirculation *10*, 259–264.

Chyla, B.J., Moreno-Miralles, I., Steapleton, M.A., Thompson, M.A., Bhaskara, S., Engel, M., and Hiebert, S.W. (2008). Deletion of Mtg16, a target of t(16;21), alters hematopoietic progenitor cell proliferation and lineage allocation. Mol. Cell. Biol. *28*, 6234–6247.

Dewald, O., Zymek, P., Winkelmann, K., Koerting, A., Ren, G., Abou-Khamis, T., Michael, L.H., Rollins, B.J., Entman, M.L., and Frangogiannis, N.G. (2005). CCL2/Monocyte Chemoattractant Protein-1 regulates inflammatory responses critical to healing myocardial infarcts. Circ. Res. *96*, 881–889.

Dutta, P., Courties, G., Wei, Y., Leuschner, F., Gorbatov, R., Robbins, C.S., Iwamoto, Y., Thompson, B., Carlson, A.L., Heidt, T., et al. (2012). Myocardial infarction accelerates atherosclerosis. Nature *487*, 325–329.

Epelman, S., Lavine, K.J., Beaudin, A.E., Sojka, D.K., Carrero, J.A., Calderon, B., Brija, T., Gautier, E.L., Ivanov, S., Satpathy, A.T., et al. (2014). Embryonic and adult-derived resident cardiac macrophages are maintained through distinct mechanisms at steady state and during inflammation. Immunity *40*, 91–104.

Essers, M.A., Offner, S., Blanco-Bose, W.E., Waibler, Z., Kalinke, U., Duchosal, M.A., and Trumpp, A. (2009). IFNalpha activates dormant haematopoietic stem cells in vivo. Nature *458*, 904–908.

Glauche, I., Moore, K., Thielecke, L., Horn, K., Loeffler, M., and Roeder, I. (2009). Stem cell proliferation and quiescence—two sides of the same coin. PLoS Comput. Biol. *5*, e1000447.

Hardesty, B., Hutton, J.J., Arlinghaus, R., and Schweet, R. (1963). Polyribosome formation and hemoglobin synthesis. Proc. Natl. Acad. Sci. USA *50*, 1078–1085.

Hofmann, W.K., de Vos, S., Komor, M., Hoelzer, D., Wachsman, W., and Koeffler, H.P. (2002). Characterization of gene expression of CD34+ cells from normal and myelodysplastic bone marrow. Blood *100*, 3553–3560.

Irizarry, R.A., Hobbs, B., Collin, F., Beazer-Barclay, Y.D., Antonellis, K.J., Scherf, U., and Speed, T.P. (2003). Exploration, normalization, and summaries of high density oligonucleotide array probe level data. Biostatistics *4*, 249–264.

Kho, A.T., Zhao, Q., Cai, Z., Butte, A.J., Kim, J.Y., Pomeroy, S.L., Rowitch, D.H., and Kohane, I.S. (2004). Conserved mechanisms across development and tumorigenesis revealed by a mouse development perspective of human cancers. Genes Dev. *18*, 629–640.

Konuma, T., Nakamura, S., Miyagi, S., Negishi, M., Chiba, T., Oguro, H., Yuan, J., Mochizuki-Kashio, M., Ichikawa, H., Miyoshi, H., Vidal, M., and Iwama, A. (2011). Forced expression of the histone demethylase Fbxl10 maintains self-renewing hematopoietic stem cells. Exp. Hematol. *39*, 697–709.e5.

Leuschner, F., Dutta, P., Gorbatov, R., Novobrantseva, T.I., Donahoe, J.S., Courties, G., Lee, K.M., Kim, J.I., Markmann, J.F., Marinelli, B., et al. (2011). Therapeutic siRNA silencing in inflammatory monocytes in mice. Nat. Biotechnol. *29*, 1005–1010.

Leuschner, F., Rauch, P.J., Ueno, T., Gorbatov, R., Marinelli, B., Lee, W.W., Dutta, P., Wei, Y., Robbins, C., Iwamoto, Y., et al. (2012). Rapid monocyte kinetics in acute myocardial infarction are sustained by extramedullary monocytopoiesis. J. Exp. Med. *209*, 123–137.

Libby, P. (2002). Inflammation in atherosclerosis. Nature *420*, 868–874.

Lo Celso, C., Fleming, H.E., Wu, J.W., Zhao, C.X., Miake-Lye, S., Fujisaki, J., Côté, D., Rowe, D.W., Lin, C.P., and Scadden, D.T. (2009). Live-animal tracking of individual haematopoietic stem/progenitor cells in their niche. Nature *457*, 92–96.

Massberg, S., Schaerli, P., Knezevic-Maramica, I., Köllnberger, M., Tubo, N., Moseman, E.A., Huff, I.V., Junt, T., Wagers, A.J., Mazo, I.B., and von Andrian, U.H. (2007). Immunosurveillance by hematopoietic progenitor cells trafficking through blood, lymph, and peripheral tissues. Cell *131*, 994–1008.

Méndez-Ferrer, S., Lucas, D., Battista, M., and Frenette, P.S. (2008). Haematopoietic stem cell release is regulated by circadian oscillations. Nature *452*, 442–447.

Moore, K.J., and Tabas, I. (2011). Macrophages in the pathogenesis of atherosclerosis. Cell *145*, 341–355.

Morrison, S.J., and Scadden, D.T. (2014). The bone marrow niche for haematopoietic stem cells. Nature *505*, 327–334.

Mossadegh-Keller, N., Sarrazin, S., Kandalla, P.K., Espinosa, L., Stanley, E.R., Nutt, S.L., Moore, J., and Sieweke, M.H. (2013). M-CSF instructs myeloid lineage fate in single haematopoietic stem cells. Nature *497*, 239–243.

Nahrendorf, M., Pittet, M.J., and Swirski, F.K. (2010). Monocytes: protagonists of infarct inflammation and repair after myocardial infarction. Circulation *121*, 2437–2445.

Nombela-Arrieta, C., Pivarnik, G., Winkel, B., Canty, K.J., Harley, B., Mahoney, J.E., Park, S.Y., Lu, J., Protopopov, A., and Silberstein, L.E. (2013). Quantitative imaging of haematopoietic stem and progenitor cell localization and hypoxic status in the bone marrow microenvironment. Nat. Cell Biol. *15*, 533–543.

Oguro, H., Ding, L., and Morrison, S.J. (2013). SLAM family markers resolve functionally distinct subpopulations of hematopoietic stem cells and multipotent progenitors. Cell Stem Cell *13*, 102–116.

Okuda, T., Nishimura, M., Nakao, M., and Fujita, Y. (2001). RUNX1/AML1: a central player in hematopoiesis. Int. J. Hematol. *74*, 252–257.

Purton, L.E., and Scadden, D.T. (2007). Limiting factors in murine hematopoietic stem cell assays. Cell Stem Cell *1*, 263–270.

Reya, T., Morrison, S.J., Clarke, M.F., and Weissman, I.L. (2001). Stem cells, cancer, and cancer stem cells. Nature *414*, 105–111.

Robbins, C.S., Chudnovskiy, A., Rauch, P.J., Figueiredo, J.L., Iwamoto, Y., Gorbatov, R., Etzrodt, M., Weber, G.F., Ueno, T., van Rooijen, N., et al. (2012). Extramedullary hematopoiesis generates Ly-6C(high) monocytes that infiltrate atherosclerotic lesions. Circulation *125*, 364–374.

Semerad, C.L., Mercer, E.M., Inlay, M.A., Weissman, I.L., and Murre, C. (2009). E2A proteins maintain the hematopoietic stem cell pool and promote the maturation of myelolymphoid and myeloerythroid progenitors. Proc. Natl. Acad. Sci. USA *106*, 1930–1935.

Serbina, N.V., and Pamer, E.G. (2006). Monocyte emigration from bone marrow during bacterial infection requires signals mediated by chemokine receptor CCR2. Nat. Immunol. *7*, 311–317.

Shi, C., Jia, T., Mendez-Ferrer, S., Hohl, T.M., Serbina, N.V., Lipuma, L., Leiner, I., Li, M.O., Frenette, P.S., and Pamer, E.G. (2011). Bone marrow mesenchymal stem and progenitor cells induce monocyte emigration in response to circulating toll-like receptor ligands. Immunity *34*, 590–601.

Shields, A.F., Grierson, J.R., Dohmen, B.M., Machulla, H.J., Stayanoff, J.C., Lawhorn-Crews, J.M., Obradovich, J.E., Muzik, O., and Mangner, T.J. (1998). Imaging proliferation in vivo with [F-18]FLT and positron emission tomography. Nat. Med. *4*, 1334–1336.

Si, Y., Tsou, C.L., Croft, K., and Charo, I.F. (2010). CCR2 mediates hematopoietic stem and progenitor cell trafficking to sites of inflammation in mice. J. Clin. Invest. *120*, 1192–1203.

Subramanian, A., Tamayo, P., Mootha, V.K., Mukherjee, S., Ebert, B.L., Gillette, M.A., Paulovich, A., Pomeroy, S.L., Golub, T.R., Lander, E.S., and Mesirov, J.P. (2005). Gene set enrichment analysis: a knowledge-based approach for interpreting genome-wide expression profiles. Proc. Natl. Acad. Sci. USA *102*, 15545–15550.

Summers, A.R., Fischer, M.A., Stengel, K.R., Zhao, Y., Kaiser, J.F., Wells, C.E., Hunt, A., Bhaskara, S., Luzwick, J.W., Sampathi, S., et al. (2013). HDAC3 is essential for DNA replication in hematopoietic progenitor cells. J. Clin. Invest. *123*, 3112–3123.

Swirski, F.K., and Nahrendorf, M. (2013). Leukocyte behavior in atherosclerosis, myocardial infarction, and heart failure. Science *339*, 161–166.

Swirski, F.K., Pittet, M.J., Kircher, M.F., Aikawa, E., Jaffer, F.A., Libby, P., and Weissleder, R. (2006). Monocyte accumulation in mouse atherogenesis is progressive and proportional to extent of disease. Proc. Natl. Acad. Sci. USA *103*, 10340–10345.

Swirski, F.K., Nahrendorf, M., Etzrodt, M., Wildgruber, M., Cortez-Retamozo, V., Panizzi, P., Figueiredo, J.L., Kohler, R.H., Chudnovskiy, A., Waterman, P., et al. (2009). Identification of splenic reservoir monocytes and their deployment to inflammatory sites. Science *325*, 612–616.

Tacke, F., Alvarez, D., Kaplan, T.J., Jakubzick, C., Spanbroek, R., Llodra, J., Garin, A., Liu, J., Mack, M., van Rooijen, N., et al. (2007). Monocyte subsets differentially employ CCR2, CCR5, and CX3CR1 to accumulate within atherosclerotic plaques. J. Clin. Invest. *117*, 185–194.

Takizawa, H., Regoes, R.R., Boddupalli, C.S., Bonhoeffer, S., and Manz, M.G. (2011). Dynamic variation in cycling of hematopoietic stem cells in steady state and inflammation. J. Exp. Med. *208*, 273–284.

Tusher, V.G., Tibshirani, R., and Chu, G. (2001). Significance analysis of microarrays applied to the ionizing radiation response. Proc. Natl. Acad. Sci. USA *98*, 5116–5121.

Wilson, A., Laurenti, E., Oser, G., van der Wath, R.C., Blanco-Bose, W., Jaworski, M., Offner, S., Dunant, C.F., Eshkind, L., Bockamp, E., et al. (2008). Hematopoietic stem cells reversibly switch from dormancy to self-renewal during homeostasis and repair. Cell *135*, 1118–1129.

Yamamoto, R., Morita, Y., Ooehara, J., Hamanaka, S., Onodera, M., Rudolph, K.L., Ema, H., and Nakauchi, H. (2013). Clonal analysis unveils self-renewing lineage-restricted progenitors generated directly from hematopoietic stem cells. Cell *154*, 1112–1126.

Yang, L., Bryder, D., Adolfsson, J., Nygren, J., Månsson, R., Sigvardsson, M., and Jacobsen, S.E. (2005). Identification of Lin(-)Sca1(+)kit(+)CD34(+)Flt3-short-term hematopoietic stem cells capable of rapidly reconstituting and rescuing myeloablated transplant recipients. Blood *105*, 2717–2723.

Young, J.C., Wu, S., Hansteen, G., Du, C., Sambucetti, L., Remiszewski, S., O'Farrell, A.M., Hill, B., Lavau, C., and Murray, L.J. (2004). Inhibitors of histone deacetylases promote hematopoietic stem cell self-renewal. Cytotherapy *6*, 328–336.

Yvan-Charvet, L., Pagler, T., Gautier, E.L., Avagyan, S., Siry, R.L., Han, S., Welch, C.L., Wang, N., Randolph, G.J., Snoeck, H.W., and Tall, A.R. (2010). ATP-binding cassette transporters and HDL suppress hematopoietic stem cell proliferation. Science *328*, 1689–1693.